LATTICE-TO-TOTAL THERMAL CONDUCTIVITY RATIO: A PHONON-GLASS ELECTRON-CRYSTAL DESCRIPTOR FOR DATA-DRIVEN THERMOELECTRIC DESIGN

A PREPRINT

Yifan Sun *
Kyoto University

Zhi Li *
Northwestern University

Tetsuya Imamura Osaka University Yuji Ohishi Osaka University

Chris Wolverton †
Northwestern University

Ken Kurosaki ‡ Kyoto University

November 27, 2025

ABSTRACT

Thermoelectrics (TEs) are promising candidates for energy harvesting with performance quantified by figure of merit, ZT. To accelerate the discovery of high-ZT materials, efforts have focused on identifying compounds with low thermal conductivity κ . Using a curated dataset of 71,913 entries, we show that high-ZT materials reside not only in the low- κ regime but also cluster near a lattice-to-total thermal conductivity ratio ($\kappa_{\rm L}/\kappa$) of approximately 0.5, consistent with the phonon-glass electron-crystal design concept. Building on this insight, we construct a framework consisting of two machine learning models for the lattice and electronic components of thermal conductivity that jointly provide both κ and $\kappa_{\rm L}/\kappa$ for screening and guiding the optimization of TE materials. Among 104,567 compounds screened, our models identify 2,522 ultralow- κ candidates. Follow-up case studies demonstrate that this framework can reliably provide optimization strategies by suggesting new dopants and alloys that shift pristine materials toward the $\kappa_{\rm L}/\kappa$ approaching 0.5 regime. Ultimately, by integrating rapid screening with PGEC-guided optimization, our data-driven framework effectively bridges the critical gap between materials discovery and performance enhancement.

Keywords Thermoelectrics · Thermal conductivity · Machine learning

1 Introduction

More than half of global primary energy consumption is ultimately lost after conversion, much of it as low-to medium-grade heat from industrial processes, transportation, and power generation [1, 2]. Recovering even a modest portion of this waste heat could significantly improve overall energy efficiency and contribute to sustainability goals. Thermoelectric (TE) materials, which can directly convert heat into electricity, are therefore attractive candidates for waste-heat harvesting in applications ranging from automotive systems to industrial plants [3, 4]. The conversion efficiency of TE materials is commonly evaluated using the dimensionless figure of merit ZT, defined as

$$ZT = \frac{S^2 \sigma}{\kappa_{\rm L} + \kappa_{\rm e}} T,\tag{1}$$

where S is the Seebeck coefficient, σ is the electrical conductivity, T is the absolute temperature, and $\kappa_{\rm L}$ and $\kappa_{\rm e}$ are the lattice and carrier contributions to the total thermal conductivity κ . A high ZT requires a large power factor $PF = S^2 \sigma$

^{*}These authors contributed equally to this work.

[†]Correspondence to: c-wolverton@northwestern.edu

[‡]Correspondence to: kurosaki.ken.6n@kyoto-u.ac.jp

and a low κ . However, optimizing TE performance is challenging because these transport parameters are strongly interrelated, and improving one often comes at the expense of another. These intricate relationships make it difficult to identify high-ZT materials through conventional trial-and-error experimentation, and have motivated data-driven strategies, particularly machine learning (ML), to guide the search and design of TE materials more efficiently.

In recent years, a number of ML models have been developed to predict the ZT of materials directly [5, 6, 7, 8, 9]. However, because ZT is a composite metric that is sensitive to carrier concentration, much of the ML effort has shifted toward predicting individual TE properties rather than ZT itself. Models have been trained to predict quantities such as the Seebeck coefficient S [5, 10, 11, 12] and the thermal conductivity κ , especially its lattice component κ_L [5, 13, 14, 15, 16]. In particular, an intrinsically low κ_L is often used as a key indicator of a promising TE material, since κ_L is largely dictated by crystal structure and bonding and is less dependent on carrier concentration than S or σ . For example, Wang et al. [14] used computed κ_L values from AFLOW to train an XGBoost model and identified several low- κ candidate materials that were subsequently validated by first-principles calculations. Barua et al. [15] developed ML models to predict κ using the Starrydata database of experimental thermoelectric measurements. More recently, Li et al. [16] trained a neural network on first-principles κ_L data and screened over 32,000 compounds from the Inorganic Crystal Structure Database (ICSD), discovering numerous additional low- κ candidates.

Still, finding a material with intrinsically low thermal conductivity is only a first step toward achieving a high ZT. In practice, most TE materials require further optimization, such as defect engineering [17, 18], band structure engineering [19, 20], and nanostructuring [21, 22], in order to boost electrical transport while further suppressing lattice thermal transport. The accumulated lessons from decades of such optimization efforts are encapsulated in the phonon-glass electron-crystal (PGEC) paradigm [23, 24, 25, 26], which calls for materials that conduct heat like a glass (suppressing phonon mobility) but conduct electrons like a crystal (enhancing carrier mobility). In essence, the PGEC concept emphasizes that an ideal thermoelectric should strike a balance between phonon and carrier transport properties. However, existing data-driven studies have largely neglected the explicit incorporation of a PGEC-based metric when screening for promising TE materials.

To address this gap in the literature and move beyond simply screening for materials with low κ or κ_L , we adopt a data-driven approach to explicitly quantify the PGEC concept in terms of the balance between phonon and carrier thermal transport. We first curate a large experimental dataset of thermoelectric properties from the Starrydata [27] repository and calculate the lattice (κ_L) and electronic thermal conductivity (κ_e) for each entry in a consistent manner. Here, κ_L reflects phonon transport, while κ_e serves as a proxy for carrier transport. Statistical analysis reveals that existing high-ZT TE materials not only lie in the low- κ regime ($\kappa \leq 2~{\rm W\,m^{-1}\,K^{-1}}$) but, more importantly, have κ_L/κ values clustering near 0.5. Further investigation into two representative TE families shows that, after the initial screening with κ , κ_L/κ acts as a valuable descriptor for designing optimization strategies toward the PGEC ideal, where $\kappa_L/\kappa \approx 0.5$.

Consequently, to incorporate this PGEC-based descriptor into the screening and optimization of thermoelectric materials, we train two ML models, one to predict $\kappa_{\rm L}$ and another to predict $\kappa_{\rm e}$ from a set of composition descriptors [28] and temperature. These models allow us to obtain both κ and $\kappa_{\rm L}/\kappa$, capture more granular information on phonon versus carrier thermal transport. To demonstrate the practical utility of our approach, we apply the trained models to screen 104,567 inorganic compounds from the Materials Project database [29] and identify 2,522 thermodynamically stable semiconductors with low thermal conductivity ($\kappa \le 2~{\rm W~m^{-1}~K^{-1}}$) at 300 K. Follow-up case studies on randomly selected candidates verify our predicted thermal condutivities using the latest published experiment results, lending credence to our models' performance beyond the test set. Beyond screening, to illustrate how the models can guide materials optimization, we select three representative candidates and, using the $\kappa_{\rm L}/\kappa \to 0.5$ design rule, propose specific dopants or alloying modifications that could tune these materials closer to the PGEC ideal. Overall, our datadriven framework, built on $\kappa_{\rm L}$ and $\kappa_{\rm e}$ models, not only enables the rapid identification of TE materials with intrinsically low thermal conductivity but also provides data-driven suggestions for optimizing those materials guided by the PGEC descriptor $\kappa_{\rm L}/\kappa$, thereby helping to bridge the gap between materials discovery and performance enhancement.

2 Methods

2.1 Data curation

We used the 2025-07-01 version of the Starrydata database [27], which contains 202,178 digitized curves (an excerpt is shown in Table 1). From these records, we retained samples (identified by sample-id) that reported a complete set of thermoelectric properties: S, σ , κ , and ZT. We then removed samples with invalid compositions or duplicate curves for any of these properties as a basic quality-control step. After confirming unit consistency across the retained records, we removed entries with implausible values, such as negative T, κ , or σ . We also removed entries with ZT > 3, since

[0.35, 0.57, 0.84]

[1416.0, 1192.0, 1034.0]

such values are extraordinarily rare for bulk thermoelectrics and too sparse to influence data visualization and model training, while sometimes reflecting human input errors in the database.

Composition	Prop-x	Prop-y	Unit-x	Unit-y	x	у
$In_{0.3}Co_4Sb_{12}$	T	S	K	$\mu { m V~K^{ ext{-}1}}$	[323.3, 418.7, 518.5]	[-163.3, -185.0, -209.5]
$In_{0.3}Co_4Sb_{12}$	T	κ	K	${ m W}{ m m}^{-1}{ m K}^{-1}$	[324.3, 423.1, 521.9]	[3.50, 3.11, 2.83]
$In_{0.3}Co_4Sb_{12} \\$	T	σ	K	$\mathrm{Scm^{-1}}$	[318.5, 422.4, 519.4]	[1416.0, 1192.0, 1034.0]

[320.7, 421.7, 524.6]

Table 1: Excerpt of the Starrydata records used in this study.

In manually curated databases like Starrydata, thermoelectric properties of the same sample-id are not perfectly aligned at the same temperature, since they are extracted from plots by humans using digitization software. Small mismatches can occur during the click-and-extract process, as exemplified in the x column of Table 1. These slight temperature offsets across properties make it impossible to directly calculate κ_e and κ_L from S, σ , and κ . To resolve this, we first performed temperature alignment: for each reported ZT at a given temperature T, we searched for S, σ , and κ values for the same sample-id within a ± 5 K window around T. If multiple values were found, the one closest to T was chosen. This window is small enough that variations in the properties are typically negligible.

To further ensure internal consistency and eliminate possible labeling errors, we recomputed ZT at each reported ZTtemperature using the corresponding S, σ , and κ values, which we denote $ZT_{\rm calc}$. By definition, if all thermoelectric properties are correctly extracted from the published figures, $ZT_{\rm calc}$ should match the author-reported ZT. Therefore, we excluded entries for which $ZT_{\rm calc}$ deviated from ZT by more than 10%. This "ZT consistency" check is also the main reason for retaining only samples with a complete set of thermoelectric properties, as mentioned earlier.

Table 2 shows the temperature-aligned data corresponding to Table 1. In this example, temperature alignment fails at $T=524.6~{
m K}$ because the closest Seebeck coefficient data (at $T=518.5~{
m K}$) lies outside the $\pm 5~{
m K}$ window, so that row is flagged for removal. After temperature alignment, we computed $ZT_{\rm calc}$ and confirmed that the remaining two entries at T = 320.7 and 421.7 K show consistent $ZT_{\rm calc}$ and ZT. Some examples of removed records with a relative difference from the reported ZT exceeding 10% are provided in the Supplementary Information (Table S1).

Table 2: Temperature-aligned records corresponding to the example in Table 1.

Sample-id	Composition	T (K)	$S \\ (\mu V K^{-1})$	$(W m^{-1} K^{-1})$	σ (S cm ⁻¹)	ZT	$ZT_{ m calc}$
5422	$In_{0.3}Co_4Sb_{12} \\$	320.7	-163.3	3.50	1416.0	0.35	0.35
5422	$In_{0.3}Co_4Sb_{12}$	421.7	-185.0	3.11	1192.0	0.57	0.55
5422	$In_{0.3}Co_4Sb_{12} \\$	524.6	-	2.83	1034.0	0.84	-

2.2 Lattice and carrier thermal conductivity calculations

Sample-id

 $In_{0.3}Co_4Sb_{12} \\$

5422

5422

5422

5422

To avoid data skewness, we further restricted the dataset to the range 300 < T < 800 K and $\kappa < 10$ W m⁻¹ K⁻¹. This window corresponds to the temperature and thermal conductivity range most commonly studied in thermoelectric research and also contains nearly all of the curated data. Total thermal conductivity κ was then split into lattice thermal conductivity (κ_L) and carrier thermal conductivity (κ_e) using the Wiedemann–Franz law:

$$\kappa_{\rm L} = \kappa - \kappa_{\rm e},$$
(2)

$$\kappa_{\rm e} = L \, \sigma \, T, \tag{3}$$

where L is the Lorenz number (in $10^{-8}~{\rm W}\,\Omega\,{\rm K}^{-2}$), estimated from S (in $\mu{\rm V}\,{\rm K}^{-1}$) using:

$$L = 1.5 + \exp[-\frac{|S|}{116}] \tag{4}$$

This approximation is typically accurate within \sim 5% for semiconductors satisfying the single parabolic band (SPB) model and within $\sim 20\%$ for more complex systems [30]. To further assess the accuracy of our calculated κ_e , we compared them with a subset of 27,698 Starrydata entries containing literature-reported κ_e values in Figure S1. Overall, we observed excellent agreement between our calculated κ_e and the literature values, with $R^2 = 0.96$ and a mean absolute difference of $0.09 \text{ W m}^{-1} \text{ K}^{-1}$.

Notably, we found that a substantial fraction of the discrepancy originates from oversimplifications in earlier works that use approximate, constant Lorenz numbers [31, 32, 33, 34, 35, 36, 37, 38]. The conclusions of some studies on thermal conductivity could change significantly if their analyses were repeated using our Lorenz numbers, which correctly account for the correlation with S, further emphasizing the importance of constructing a uniform and consistent dataset. Nevertheless, even in cases where our calculated thermal conductivities match well with the reported values, there are anomalous cases where $\kappa_{\rm L}$ or $\kappa_{\rm e}$ approaches zero. These anomalies can be attributed to breakdowns of the SPB model due to phase impurities [39, 40], phase metastability and transitions [41], or extremely complex transport behavior [42]. Given that there is no other generally applicable approach to calculate $\kappa_{\rm L}$ and $\kappa_{\rm e}$, and the rarity of these cases, we retain these data points in our dataset for future investigation. A more detailed discussion of the uncertainties in $\kappa_{\rm L}$ and $\kappa_{\rm e}$ can be found in the Supplementary Information.

2.3 Machine learning framework

The final curated dataset contains 71,913 entries, which we split into training (80%) and test (20%) sets while avoiding composition overlap. Specifically, we perform a group-based split so that all entries sharing the same reduced formula are assigned to the same set, preventing any reduced formula from appearing in both sets. Figure S2 shows examples of the temperature-dependent ZT and κ in the final dataset.

Each composition in Table 2 was featurized using its Magpie chemical descriptors [28] together with the measurement temperature, yielding an initial set of 133 features for predicting lattice ($\kappa_{\rm L}$) and electronic ($\kappa_{\rm e}$) thermal conductivities. Features with zero variance across the training data were first removed, followed by a Pearson correlation analysis on the remaining features. For any pair with an absolute correlation coefficient greater than 0.99, one of the two features was removed. The correlated feature pairs and the features removed are listed in the Supplementary Information. Feature removal was performed exclusively on the training set to prevent information leakage, and the resulting feature set was then applied to the test set. The final feature set used for training contains 108 features in total, consisting of 107 Magpie descriptors and the temperature.

We evaluated four tree-based algorithms (XGBoost, LightGBM, Random Forest, and CatBoost), chosen for their strong performance in previous studies [7, 14, 15]. Model performance was assessed using 5-fold GroupKFold cross-validation, grouping by reduced formula to ensure no composition overlap among folds. The primary metric for model selection was the mean absolute error (MAE), chosen for its interpretability and reduced sensitivity to outliers. The model with the lowest cross-validated MAE was then further tuned using GridSearchCV, retrained on the full training set, and finally evaluated on the independent test set. In addition, to provide a baseline for performance comparison, we also trained a single model to directly predict the total thermal conductivity κ . This baseline model allows us to assess whether predicting the two components ($\kappa_{\rm L}$ and $\kappa_{\rm e}$), while providing more granular information on transport properties, comes at the cost of reduced accuracy in κ compared with a model trained directly on total thermal conductivity. Details of this baseline model are provided in the Supplementary Information.

3 Results and Discussion

3.1 Data overview

As mentioned in the Introduction, thermal conductivity, particularly the lattice component κ_L , has long served as a primary descriptor in the search for promising thermoelectric materials. Most TE compounds are semiconductors with intrinsically small electronic thermal conductivity κ_e , so a low κ_L (or equivalently, low κ) has traditionally been regarded as an intrinsic indicator of high thermoelectric potential. However, materials exhibiting intrinsically low κ_L only provide a promising starting point. The subsequent optimization pathway needed to approach the PGEC regime, which is crucial from an experimentalist's point of view, is not captured in most existing studies.

The emergence of the Starrydata [27] repository offers a unique opportunity to address this gap, as it aggregates hundreds of thousands of experimentally measured samples, including both pristine compounds and a wide range of doped and alloyed derivatives. This breadth allows, for the first time at scale, direct tracking of how key thermoelectric properties evolve under chemical modification and how these modifications influence ZT. Because interpreting the high-dimensional and strongly coupled relationships among S, σ , κ , and ZT is challenging, we focus our data-driven analysis on thermal conductivity and its components to gain systematic insights into how chemical modifications steer materials toward or away from the thermoelectric optimum.

First, we visualize the ZT distribution with respect to $\kappa_{\rm e}$ and $\kappa_{\rm L}$ in Figure 1(a). For samples with approximately the same total thermal conductivity κ , the highest attainable ZT tends to occur within a limited range of $\kappa_{\rm e}$ and $\kappa_{\rm L}$. To better clarify their relative contributions, we next plot ZT with respect to the lattice-to-total thermal conductivity ratio $\kappa_{\rm L}/\kappa$ in Figure 1(b). Across the full dataset, ZT varies with $\kappa_{\rm L}/\kappa$ in an inverted-U-shaped manner, with most data points

lying in the $\kappa_{\rm L}/\kappa \approx 0.9$ –1.0 range, while the highest ZT values occur around $\kappa_{\rm L}/\kappa \approx 0.5$. From Figures S4(a) and (b), we further confirm that the dominance of $\kappa_{\rm L}$ (with $\kappa_{\rm L}/\kappa$ close to 1) is present in both pristine and optimized samples, reflecting the typical behavior of non-degenerate semiconductors in which lattice thermal conductivity dominates. In contrast, the emergence of high ZT near $\kappa_{\rm L}/\kappa \approx 0.5$ is evident only in the optimized samples, consistent with deliberate optimization efforts to enhance the carrier contribution while suppressing phonon transport. When we further divide the data by κ , as shown in Figure S4(c), the characteristic $\kappa_{\rm L}/\kappa$ range associated with high ZT shifts toward 0.5 as κ decreases, indicating that the most successful optimizations drive materials toward a regime where $\kappa_{\rm L}$ and $\kappa_{\rm e}$ contribute comparably to the total thermal conductivity.

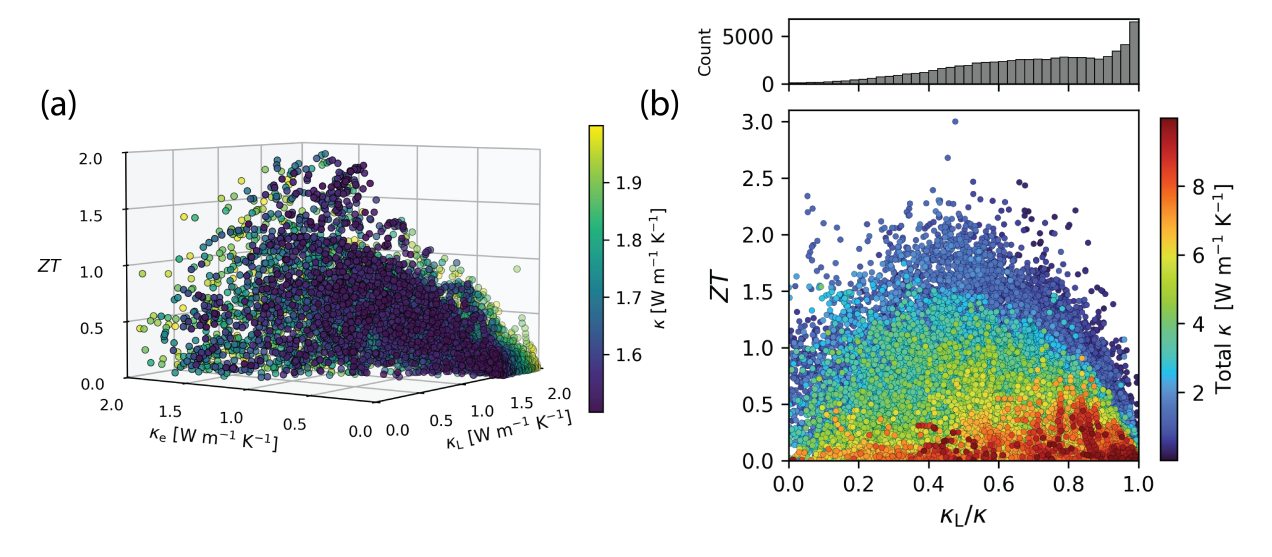


Figure 1: Relationships between ZT and thermal conductivity in the literature from Starrydata. (a) shows the relation between ZT, $\kappa_{\rm L}$, and $\kappa_{\rm e}$ at approximately fixed total κ . (b) shows ZT versus $\kappa_{\rm L}/\kappa$ (lattice-to-total thermal conductivity ratio) for the full curated dataset.

To illustrate more concretely how the tendency toward $\kappa_{\rm L}/\kappa \to 0.5$ reflects optimization toward the PGEC regime, we next examine the distribution of ZT with respect to $\kappa_{\rm L}/\kappa$ before and after optimization in two representative families, CoSb₃ and GeTe (Figure 2). Details of the family classification are provided in the Supplementary Information.

CoSb₃, a typical non-degenerate semiconductor. Figure 2(a) shows that unfilled skutterudites, CoSb₃, mostly have ZT below 0.5 with $\kappa_{\rm L}/\kappa$ in the 0.6–1.0 range. This is because pristine CoSb₃ exhibits typical non-degenerate semiconductor behavior with low intrinsic carrier concentrations (10^{17} – 10^{18} cm⁻³), and therefore a small $\kappa_{\rm e}$ [43, 44]. In addition, single-crystalline CoSb₃ has a relatively high intrinsic lattice thermal conductivity of $\kappa_{\rm L} \sim 10~{\rm W~m^{-1}~K^{-1}}$ [45]. Consequently, the corresponding optimization strategy follows the usual thermoelectric playbook, reducing $\kappa_{\rm L}$ while maintaining or improving electrical transport, which indirectly appears as a reduction in $\kappa_{\rm L}/\kappa$. As a result, optimized CoSb₃ samples show reduced κ and $\kappa_{\rm L}/\kappa$ values that move closer to 0.5.

Park et al. [46] provide a representative example of the outlined strategy by filling CoSb₃ with Yb. The intrinsic CoSb₃ sample (sample-id 4428) is a p-type semiconductor with a hole concentration of 2.56×10^{18} cm⁻³. Adding a small amount of Yb yields Yb_{0.2}CoSb₃ (sample-id 4430), which becomes n-type with a much higher electron concentration of 2.45×10^{20} cm⁻³. At 623 K, this transformation changes S from +190 to $-200~\mu\text{V K}^{-1}$ and σ from 208 to $1024~\text{S cm}^{-1}$, and is reflected in a jump in $\kappa_{\rm e}$ from 0.22 to 1.07 W m⁻¹ K⁻¹, confirming Yb as an efficient donor in CoSb₃. At the same time, weak bonding and large mass contrast make Yb act as a rattler in the CoSb₃ framework, reducing $\kappa_{\rm L}$ from 4.60 to 2.00 W m⁻¹ K⁻¹ at 623 K. Together, these changes implement the PGEC strategy, raising the ZT of CoSb₃ from 0.1 to 0.9 at 623 K and shifting $\kappa_{\rm L}/\kappa$ from 0.95 to 0.65, toward the $\kappa_{\rm L}/\kappa \approx 0.5$ PGEC regime.

GeTe, a self-doped degenerate semiconductor. In Figure 2(b), pristine GeTe samples (before optimization) generally show κ_L/κ values smaller than 0.5. This behavior can be traced to two main factors. First, strong anharmonicity induced by the stereochemically active lone pairs on Ge leads to a relatively low κ_L [47]. Second, pristine GeTe is well known for its very high intrinsic Ge-vacancy concentration [48, 49, 50]. These native acceptors boost the hole concentration to $\sim 10^{21}$ cm⁻³, making GeTe an intrinsically degenerate semiconductor with high σ and therefore a

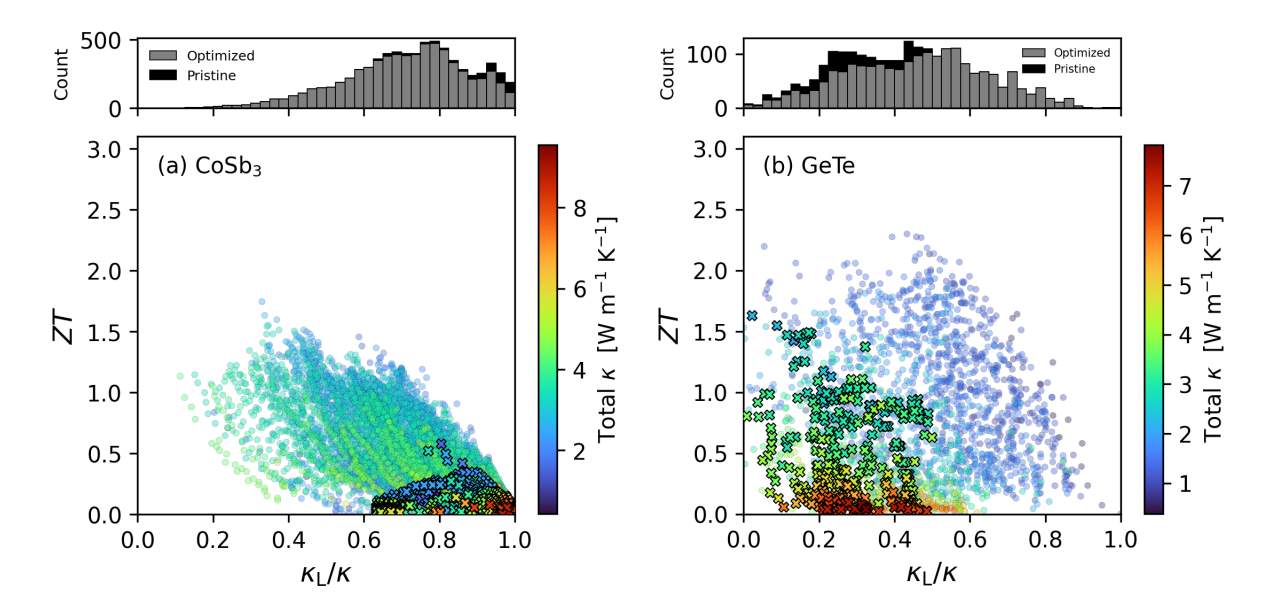


Figure 2: Relationships between ZT and the lattice-to-total thermal conductivity ratio (κ_L/κ), for two representative TE material families: (a) CoSb₃ and (b) GeTe. Pristine compositions, defined as those whose reduced formula exactly matches the corresponding stoichiometric compound (CoSb₃ or GeTe), are shown as filled crosses, while optimized variants are shown as semi-transparent circles.

large κ_e [51, 52]. However, the excessive hole concentration also results in a low S, which explains why most pristine GeTe samples in Figure 2(b) still exhibit $ZT \leq 1$.

Upon optimization, we observe significantly increased ZT accompanied by decreased κ and an increase in $\kappa_{\rm L}/\kappa$ toward 0.5. A representative example is provided by Li et al. [53], who doped Sb on the Ge site. The Sb³⁺ cations act as donors and reduce the hole concentration from 3×10^{21} cm⁻³ in pristine GeTe (sample-id 45057) to 2.2×10^{20} cm⁻³ in Ge_{0.9}Sb_{0.1}Te (sample-id 45069). The suppressed hole concentration increases S and decreases σ , shifting $\kappa_{\rm L}/\kappa$ from 0.16 to 0.39 at 750 K, closer to 0.5. The peak ZT of these two compounds increases accordingly, from 0.79 to 1.76 at 750 K.

Taken together, the statistical trends in ZT, κ , and $\kappa_{\rm L}/\kappa$ indicate that the features associated with high ZT are largely system-independent. Across both non-degenerate and degenerate thermoelectric families, most high-performance samples converge toward $\kappa_{\rm L}/\kappa \approx 0.5$ after optimization, consistent with the PGEC ideal. Thus, our data-driven analysis highlights that $\kappa_{\rm L}/\kappa$ can serve as a PGEC-based, semi-quantitative guideline for guiding further optimization once an intrinsically low- κ material has been identified in high-throughput DFT or ML screening.

3.2 Model Performances

The cross-validation results for both models (κ_L and κ_e) averaged across five folds are summarized in Table 3. For predicting both κ_L and κ_e , we selected Random Forest as the best model based on the cross-validated mean absolute error (MAE). While CatBoost offers a slightly higher R^2 when predicting electronic thermal conductivity, the improvement is marginal (less than 0.01), and its much larger hyperparameter space makes tuning computational-extensive and increases the risk of overfitting on the training data.

After model selection, the search spaces we explored and the optimal hyperparameters selected for the two Random Forest models are summarized in Table S2, and the corresponding cross-validation metrics after tuning are reported in Table 4. Hyperparameter optimization yields only modest improvements in performance for both κ_L and κ_e predictions. Nevertheless, the tuned models show test-set performance (Table 4 and Figure 3) that is consistent with the cross-validation results, indicating that hyperparameter optimization did not lead to overfitting. The parity plots in Figure 3 further show that both models perform particularly well for materials with low thermal conductivity, which constitute the majority of the training data from the Starrydata repository and are characteristic of thermoelectric materials.

While separately predicting κ_L and κ_e provides more granular insight into a material's total thermal conductivity, it raises the question of whether this decomposition degrades the accuracy of the resulting κ . This is particularly relevant

Table 3: Cross-validation performance for the lattice and electronic thermal conductivity models. Units for Mean Absolute Error (MAE) and Root Mean Squared Error (RMSE) are in W m^{-1} K⁻¹.

Model	Lattice th	nermal conducti	vity $(\kappa_{ m L})$	Electronic	Electronic thermal conductivity ($\kappa_{\rm e}$)			
1,10001	MAE	RMSE	R^2	MAE	RMSE	\mathbb{R}^2		
XGBoost	0.38	0.66	0.77	0.25	0.41	0.71		
LightGBM	0.39	0.65	0.78	0.26	0.41	0.71		
Random Forest	0.35	0.64	0.79	0.23	0.39	0.73		
CatBoost	0.37	0.63	0.79	0.24	0.39	0.74		

Table 4: Cross-validation (after tuning) and held-out test performance for the lattice and electronic thermal conductivity models. Units for MAE and RMSE are in $W\,m^{-1}\,K^{-1}$

Model	Cross-validation			Held-out test		
	MAE	RMSE	\mathbb{R}^2	MAE	RMSE	\mathbb{R}^2
Lattice thermal conductivity ($\kappa_{\rm L}$) Electronic thermal conductivity ($\kappa_{\rm e}$)	0.35 0.22	0.62 0.38	0.80 0.75	0.34 0.20	0.61 0.36	0.80 0.75

because our approach computes κ as $\kappa_L + \kappa_e$, so errors from the two models could in principle accumulate, leading to worse MAE and RMSE than a single model trained directly on total thermal conductivity. To assess this, we compared κ obtained by summing the predictions of the κ_L and κ_e models with κ predicted by a baseline model trained directly on total thermal conductivity (details in the Supplementary Information). The parity plots in Figure 4 show that the additive approach achieves an R^2 above 0.8 on the held-out test set, comparable to the baseline model. Given this comparable performance, we use $\kappa = \kappa_L + \kappa_e$ computed from the separate models for all subsequent analyses.

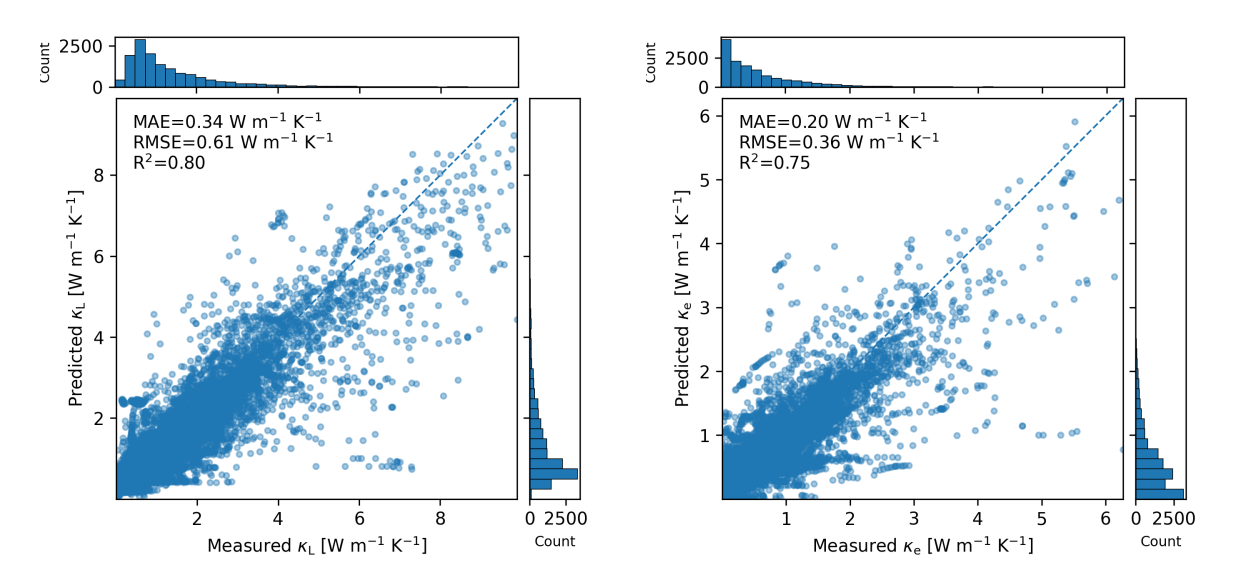


Figure 3: Fine-tuned model's performance on the held-out test set for lattice thermal conductivity $\kappa_{\rm L}$ and electronic thermal conductivity $\kappa_{\rm e}$.

Although the optimized models' performance is not outstanding, it is reasonable given that our models rely solely on elemental-level chemical descriptors (the Magpie feature set) and measurement temperature, whereas thermal conductivity is also strongly influenced by crystal structure, defects, and microstructural characteristics that are not captured in the present feature space. This is further illustrated in Figure S6, which examines the model's predictions for the well-studied compound Sb_2Te_3 . Even at the same temperature, the literature reports a wide spread of thermal conductivity values for Sb_2Te_3 prepared via different synthesis routes [54, 55, 56, 57]. While our model's predictions successfully capture both the average magnitude and the temperature dependence of the lattice and electronic thermal

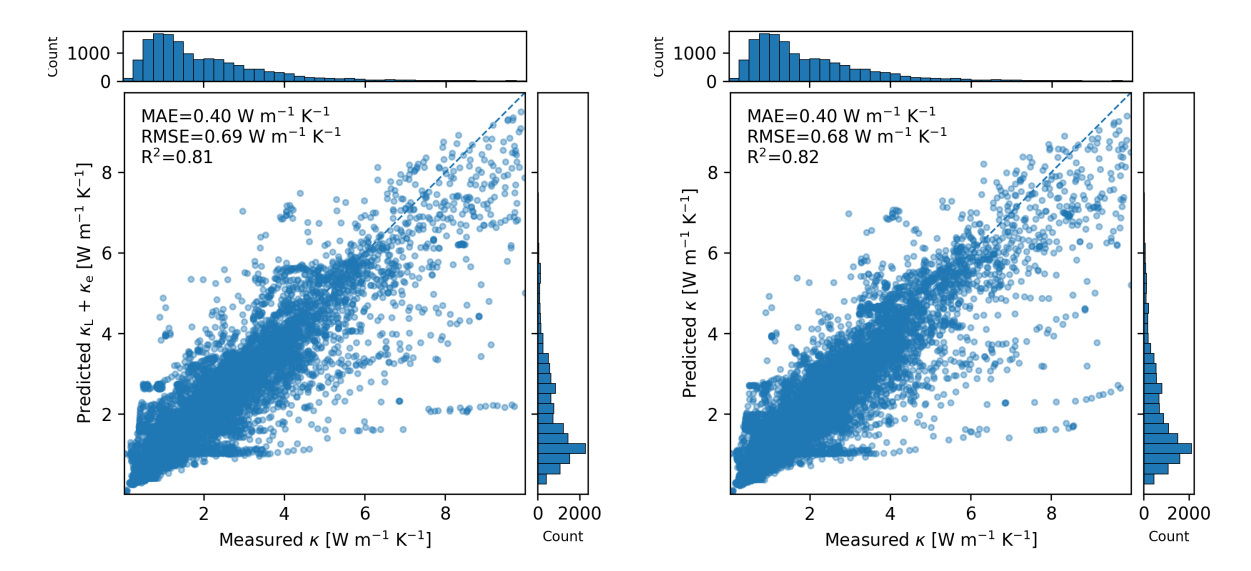


Figure 4: Performance on the held-out test set for total thermal conductivity κ obtained (a) by summing the predicted κ_L and κ_e (additive model) and (b) from a baseline model trained directly on κ .

conductivity across these Sb_2Te_3 samples, the model cannot resolve variations beyond composition and temperature that arise from structural and microstructural differences, a behavior also observed in other composition-based models [12].

The primary reason for excluding these additional structure-related descriptors is not merely the lack of recorded information in the Starrydata repository, but the inherent difficulty of obtaining such information from the literature. Thermoelectric materials typically contain complex, multi-element compositions with varying dopants or alloying elements, making automated, rule-based extraction of key compositional and structural attributes from raw chemical formulas alone extremely challenging. Although state-of-the-art large language models, such as GPT, offer a promising route for extracting doping or structural information from the literature [58, 59], this approach ultimately depends on the information being reported. In practice, doped or alloyed structures are often not comprehensively investigated and thus rarely published as Crystallographic Information Files in thermoelectric studies. For example, Itani et al. [59] found that more than half of thermoelectric-related papers in their 100-paper sample lacked basic structural features such as space groups or lattice parameters. While there are standardized structural databases, such as the ICSD and Materials Project, direct utilization of these records is impractical here because they usually correspond to idealized or undoped structures and often deviate from the actual doped or alloyed high-performance samples in our training data. For these reasons, we rely on composition-only descriptors and temperature in the present work and consider the resulting model performance for $\kappa_{\rm L}$, $\kappa_{\rm e}$, and κ sufficient for materials screening, with more accurate thermoelectric properties to be confirmed by experiments and first-principles calculations.

3.3 Feature Importance Analysis

Beyond the need to obtain κ_L to calculate the PGEC descriptor κ_L/κ , another major motivation for modeling κ_L and κ_e separately is that phonon and electron heat transport are governed by different physical mechanisms. This distinction is evident in Figure 5, where we apply SHAP analysis to probe what the models have actually learned and use it to gain chemical insight into the factors that control κ_L and κ_e .

In both models, Temperature emerges as one of the most influential features and, in most cases, higher T leads to lower predicted $\kappa_{\rm L}$ and $\kappa_{\rm e}$. This aligns with physical expectations, since increasing temperature enhances phonon–phonon (Umklapp) scattering and electron–phonon coupling, which suppress lattice heat transport and reduce σ , and therefore $\kappa_{\rm e}$ via the Wiedemann–Franz relation. For $\kappa_{\rm e}$, there is a small subset of compositions where the model's response to T is weaker or in the opposite direction, which we attribute to competition between the Lorenz number L (through its correlation with S), σ , and the explicit temperature T in $\kappa_{\rm e} = L\sigma T$. Another consistently important input is mean MeltingT, which tends to increase both $\kappa_{\rm L}$ and $\kappa_{\rm e}$. High melting points generally correlate with strong bonding, which is associated with larger phonon group velocities and higher electron densities. As a result, materials with larger mean MeltingT tend to exhibit higher predicted $\kappa_{\rm L}$ and $\kappa_{\rm e}$.

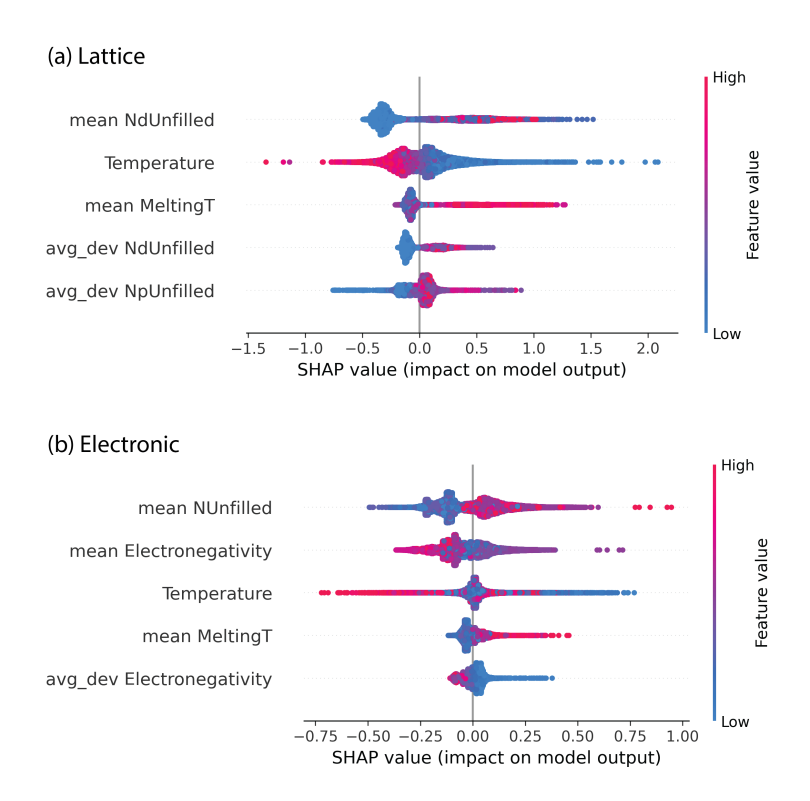


Figure 5: SHAP beeswarm plots for the (a) κ_L and (b) κ_e Random Forest models, computed on the entire training set. Features are ordered by mean |SHAP|.

For the $\kappa_{\rm L}$ model, the unfilled d-electron count, mean NdUnfilled, has an overall positive effect on $\kappa_{\rm L}$, meaning that compositions enriched in s-block and early d-block elements are predicted to have higher $\kappa_{\rm L}$. This reflects the tendency of these elements to form strong, directional s-p and d-p hybridized bonds that stiffen the lattice and increase phonon group velocities. Conversely, late d-block elements such as Cu and Ag, with fuller d shells, tend to form softer and more anharmonic bonds that hinder phonon transport. Notably, a few compositions with low mean NdUnfilled still show high $\kappa_{\rm L}$; these likely correspond to p-block-dominated chemistries such as AlN and SiC, which also possess strong bonding and thus high lattice thermal conductivity. The average deviation of unfilled d- and p-electron counts, avg dev NdUnfilled and avg dev NpUnfilled, respectively, has a more nuanced positive impact on $\kappa_{\rm L}$. These features quantify the contrast in unfilled d/p counts between constituent elements, that is, the degree of "role differentiation" or bonding complementarity between cations and anions. Larger contrast typically accompanies strong ionic-covalent hybridization and high bond stiffness, which promote higher phonon group velocity and thus higher $\kappa_{\rm L}$.

In contrast, the κ_e model highlights features that act as proxies for electron affinity and predominantly govern σ . First, the mean unfilled valence-orbital count, mean NUnfilled, has a positive impact on κ_e , since more unfilled valence states favor electronic delocalization, increase metallicity and σ , and therefore raise κ_e . Second, mean Electronegativity shows a negative impact on κ_e . Lower mean electronegativity corresponds to more metallic bonding that supplies conduction electrons, enhancing σ and κ_e , whereas higher mean electronegativity reflects stronger electron affinity and more localized electrons, which suppress carrier mobility and reduce κ_e . Finally, avg dev Electronegativity also impacts κ_e negatively. Larger inter-element electronegativity mismatch implies stronger charge transfer and more polar bonding, promoting electron localization and lowering carrier mobility, which in turn decreases κ_e . Small electronegativity contrast (near-isoelectronegativity) instead favors delocalization and more metal-like bands, increasing κ_e .

Overall, these chemical trends are in line with physical expectations, indicating that both models capture reasonable relationships between composition and lattice or electronic thermal conductivity. By jointly interpreting the κ_L and κ_e models, we obtain a chemically transparent picture of how phonon and electron transport can be differentiated and, to some extent, decoupled in thermoelectric materials. In particular, "global" levers such as temperature and overall bond strength tend to drive κ_L and κ_e in the same direction: strong, high–melting-point frameworks both stiffen the lattice and support good electronic transport. Such factors alone are not sufficient for realizing the PGEC ideal.

Instead, PGEC behavior must be approached by tuning levers that act more selectively on one transport channel. To suppress $\kappa_{\rm L}$, the lattice should be chemically softened and structurally disturbed, for example by incorporating weak-bonding atoms with minimal contrast in cation—anion valence configuration, so that the overall lattice remains soft and anharmonic. Meanwhile, increasing $\kappa_{\rm e}$ requires metallic, low-contrast electronegativity environments that support electron exchange, band formation, and long-range delocalization even in a relatively soft lattice. Mapped onto the periodic table, these requirements are most naturally satisfied by combinations of late d-block and heavier p-block elements that decouple soft bonding from high electron density. Therefore, the core chemical insight from our data-driven interpretation is that promising PGEC thermoelectrics are those in which elemental combinations decouple bond strength from electron density, enabling a phonon-glass lattice to coexist with an electron-crystal conduction network.

4 Material Screening and Optimization

Having established that the κ_L and κ_e models are reasonably accurate and chemically interpretable, we next use them for data-driven screening and optimization of thermoelectric materials. Specifically, we apply the trained models to 104,567 unique compositions from the Materials Project database [29] that are not present in the training or test sets. As shown in Figure 6(a), our initial screening focuses on binary and ternary compounds that are predicted to be thermodynamically relatively stable (energy above hull smaller than 0.1 eV/atom) and exhibit finite band gaps. Among the 14,830 compounds that satisfy these criteria, 2,522 are predicted to have low $\kappa \le 2~{\rm W\,m^{-1}\,K^{-1}}$ at 300 K and are thus promising candidates for further exploration. The predicted κ and κ_L/κ values for these 2,522 compositions are shown in Figure 6(b).

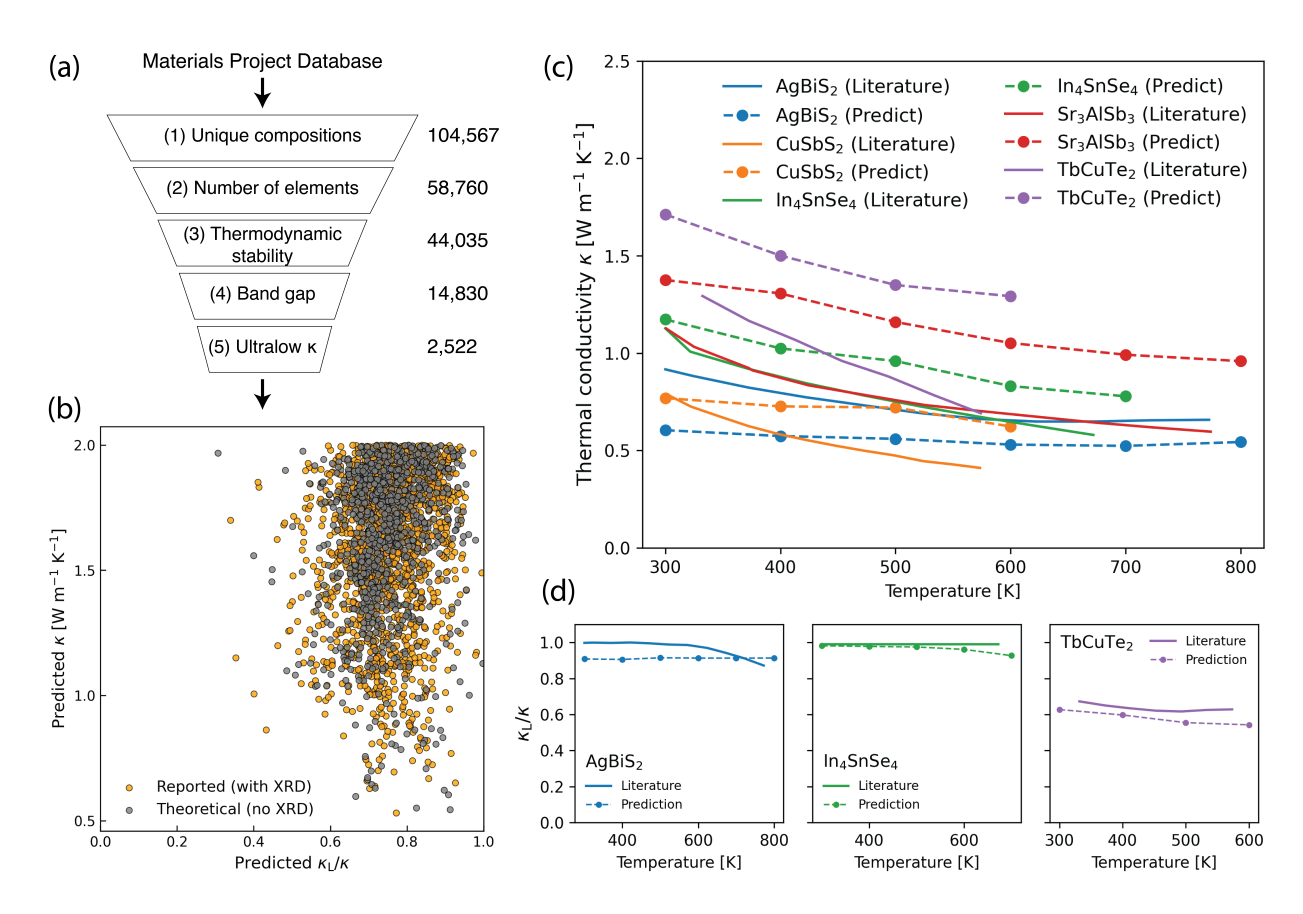


Figure 6: (a) Workflow used to screen pristine compositions with ultralow total thermal conductivity at 300 K. (b) Relationship between total thermal conductivity and lattice-to-total thermal conductivity ratio, $\kappa_{\rm L}/\kappa$, for the 2,522 promising compositions selected for further investigation. (c) and (d) Comparison between model predictions and literature values of total thermal conductivity and $\kappa_{\rm L}/\kappa$ for several compositions reported in the literature but not included in Starrydata. The overall agreement indicates that the models generalize beyond the training set.

To further evaluate our models' generalizability to unseen real-world TE materials, we randomly selected, from this set of 2,522 compounds, several reported but relatively overlooked materials (AgBiS₂ [60], CuSbS₂ [61], In₄SnSe₄ [62], Sr₃AlSb₃ [63], and TbCuTe₂ [64]) that are not recorded in Starrydata. We also confirmed that their doped variants are not included in Starrydata. For each material, we compare the predicted (dashed lines) and reported (solid lines) κ from the literature in Figure 6(c). The overall agreement is reasonably good, consistent with the MAE of approximately 0.4 W m⁻¹ K⁻¹ for our model (Figure 4). The temperature-dependent trends of all five materials are also well captured, further supporting the use of our models for screening and predicting κ of previously unseen compositions at various temperatures.

Additionally, for AgBiS₂, In₄SnSe₄, and TbCuTe₂, literature values of $\kappa_{\rm L}$ are available, which allows the lattice-to-total thermal conductivity ratio $\kappa_{\rm L}/\kappa$, the PGEC descriptor, to be calculated and compared with our predictions. As shown in Figure 6(d), the predicted $\kappa_{\rm L}/\kappa$ values are in good agreement with the reported values. Most importantly, our trained models correctly predict whether each pristine compound has $\kappa_{\rm L}/\kappa$ above or below 0.5, the key threshold we identified as separating different optimization strategies for driving materials toward the PGEC regime and thereby enhancing ZT. Based on the combination of κ and $\kappa_{\rm L}/\kappa$, it is evident that for AgBiS₂ and In₄SnSe₄, which both exhibit inherently low κ and relatively high $\kappa_{\rm L}/\kappa$, increasing $\kappa_{\rm e}$ is necessary to shift $\kappa_{\rm L}/\kappa$ toward 0.5. In contrast, TbCuTe₂ already lies near the optimal $\kappa_{\rm L}/\kappa$ ratio, so suppressing its relatively high κ while maintaining $\kappa_{\rm L}/\kappa$ becomes the priority.

To qualitatively explore how doping can be used to optimize the thermoelectric performance of these three materials, we use our $\kappa_{\rm L}$ and $\kappa_{\rm e}$ models to obtain κ and $\kappa_{\rm L}/\kappa$ for a series of doped variants, as shown in Figure 7. All predictions are performed at the temperature at which each pristine compound attains its maximum ZT in the literature [60, 62, 64], restricted to $T \leq 800$ K, where our models were trained and validated.

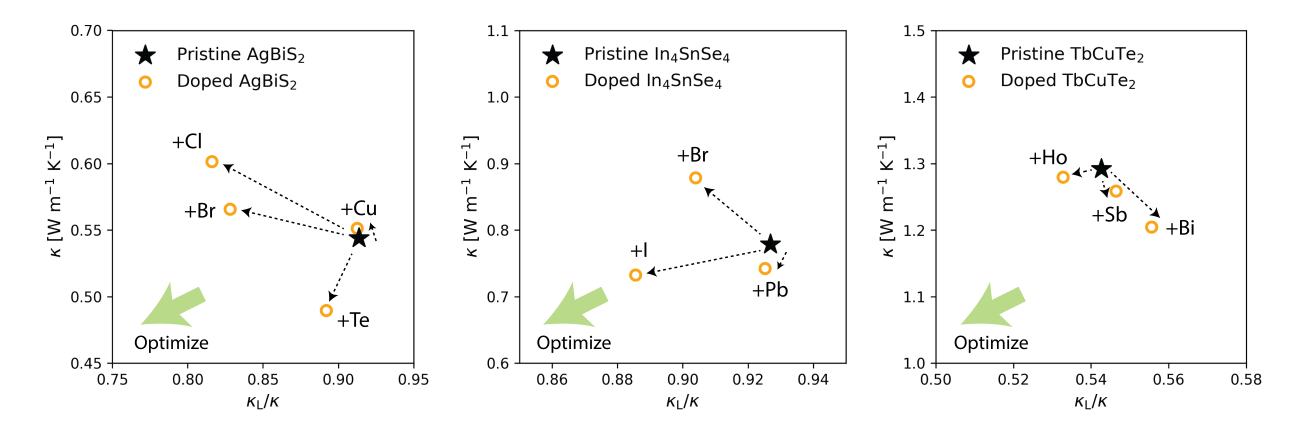


Figure 7: Predicted optimization paths for AgBiS₂ (left), In₄SnSe₄ (middle), and TbCuTe₂ (right) from the perspective of reducing κ while tuning $\kappa_{\rm L}/\kappa$ toward 0.5. Stars and open circles correspond to pristine and doped materials, respectively, and the dashed lines illustrate how selected dopants move κ and $\kappa_{\rm L}/\kappa$. The green arrow highlights the PGEC design goal of achieving $\kappa_{\rm L}/\kappa \approx 0.5$ while lowering κ .

For n-type $AgBiS_2$, experimental results already show that Cl substitution on the S site and the introduction of Cu interstitials enhance the carrier concentration and thereby decrease κ_L/κ by enhancing κ_e [60]. These trends are also reflected in our predictions in Figure 7, although our model underestimates the magnitude of the Cu-interstitial effect. We further used the model to explore how aliovalent and isovalent chalcogen-site doping with Br and Te, respectively, shape κ and κ_L/κ in $AgBiS_2$, which, to our knowledge, has not been clarified in the literature. For both dopants, the models predict a slight shift in κ_L/κ towards 0.5. In the Te case this comes mainly from an increase in Te0, whereas in the Te1 case it arises from a modest reduction in Te2 at nearly unchanged Te3, which is qualitatively consistent with physical expectations. For Te4, Te6 doping follows the reported trend [62], where Te7 doped Te8 are also in the Te8 are also in the Te9 are also in the Te9 are also in the Te9 and thus a reduced Te9, but at the expense of a slightly higher Te8. Our models suggest that, relative to Te9, heavier donor dopants such as Te9 on the Te9 on the Te9 are also interested Te9 and thus a reduced Te9 on the Te

In contrast, pristine TbCuTe₂ already lies near the optimal κ_L/κ level. Consequently, unlike AgBiS₂ and In₄SnSe₄, where the priority is to boost electronic performance, the emphasis for optimizing TbCuTe₂ should be on suppressing total thermal conductivity while maintaining κ_L/κ close to 0.5. Using our models, we qualitatively assess Sb and Bi substitution on the Te site, which is predicted to lower the overall κ but also slightly degrade κ_e . Ho substitution on the Tb site, by comparison, is expected to yield a modest reduction in κ_L/κ together with a reduced κ , consistent with the

higher electrical conductivity reported for HoCuTe₂ relative to TbCuTe₂ [64] and the additional Tb-site disorder that can reduce both κ_L and κ .

Together, these three examples highlight that our κ_L and κ_e models not only enable reliable and efficient screening of materials with low thermal conductivity, but also provide the estimate of PGEC descriptor κ_L/κ , which is critical for choosing appropriate optimization strategies for promising pristine compounds. Beyond screening, the models also offer a practical tool for qualitatively exploring elemental substitution effects on both κ and κ_L/κ , thereby guiding promising candidates toward a PGEC regime that is favorable for achieving high thermoelectric performance.

5 Conclusion

In this work, we used a large, experimentally derived thermoelectric dataset to revisit the phonon-glass electron-crystal (PGEC) concept from a quantitative, data-driven perspective by examining the lattice-to-total thermal conductivity ratio κ_L/κ across tens of thousands of measurements. We showed that high-ZT materials tend to have not only low κ but also cluster around $\kappa_L/\kappa \approx 0.5$, indicating that an approximately equal partition of thermal transport between phonons and charge carriers is a semi-quantitative signature of the PGEC regime. This trend is seen not only in the full dataset but is also validated within two representative thermoelectric families, CoSb₃ and GeTe.

Guided by these observations, we developed two composition- and temperature-based machine learning models to predict κ_L and κ_e , enabling direct evaluation of both κ and κ_L/κ in high-throughput screening. Subsequent SHAP analysis of both models provided chemically intuitive guidelines for element selection that balance electrical and phonon transport, linking specific compositional motifs to soft lattices and delocalized electron density.

Finally, we demonstrated that the trained models are predictive for a set of recently reported and underexplored compounds. They not only reproduce measured thermal conductivities and $\kappa_{\rm L}/\kappa$ but also suggest concrete optimization routes, such as specific doping or alloying elements, to tune $\kappa_{\rm L}/\kappa$ toward the PGEC target of 0.5. Overall, this work establishes $\kappa_{\rm L}/\kappa$ as a practical PGEC descriptor and incorporates it within a data-driven screening framework that provides interpretable chemical design rules, helping bridge the gap between thermoelectric materials discovery and performance optimization.

Competing interests

The authors declare no competing interests.

Author contributions

Y.S. and Z.L. conceived the research ideas. Y.S. and I.T. curated the dataset. Z.L. led the thermoelectric trend and data overview analysis. Y.S. performed additional data analysis and trained the machine learning models. Y.S. and Z.L. carried out the materials screening and optimization, and drafted the manuscript. Y.O., C.W., and K.K. supervised the research. All authors contributed to discussions and provided feedback on the manuscript.

References

- [1] Clemens Forman, Ibrahim Kolawole Muritala, Robert Pardemann, and Bernd Meyer. Estimating the global waste heat potential. *Renewable and Sustainable Energy Reviews*, 57:1568–1579, 2016.
- [2] Charles Geffroy, Drew Lilley, Pedro Sanchez Parez, and Ravi Prasher. Techno-economic analysis of waste-heat conversion. *Joule*, 5(12):3080–3096, 2021.
- [3] Lon E Bell. Cooling, heating, generating power, and recovering waste heat with thermoelectric systems. *Science*, 321(5895):1457–1461, 2008.
- [4] G Jeffrey Snyder and Eric S Toberer. Complex thermoelectric materials. *Nature Materials*, 7(2):105–114, 2008.
- [5] Gyoung S Na and Hyunju Chang. A public database of thermoelectric materials and system-identified material representation for data-driven discovery. *npj Computational Materials*, 8(1):214, 2022.
- [6] Yi Li, Jingzi Zhang, Ke Zhang, Mengkun Zhao, Kailong Hu, and Xi Lin. Large data set-driven machine learning models for accurate prediction of the thermoelectric figure of merit. *ACS Applied Materials & Interfaces*, 14(50): 55517–55527, 2022.
- [7] Nuttawat Parse and Supree Pinitsoontorn. Machine learning for predicting ZT values of high-performance thermoelectric materials in mid-temperature range. *APL Materials*, 11(8), 2023.

- [8] Nikhil K Barua, Sangjoon Lee, Anton O Oliynyk, and Holger Kleinke. Thermoelectric material performance (zT) predictions with machine learning. ACS Applied Materials & Interfaces, 17(1):1662–1673, 2024.
- [9] Yingying Xu, Xinyi Liu, and Jifen Wang. Prediction of thermoelectric-figure-of-merit based on autoencoder and light gradient boosting machine. *Journal of Applied Physics*, 135(7), 2024.
- [10] Al'ona Furmanchuk, James E Saal, Jeff W Doak, Gregory B Olson, Alok Choudhary, and Ankit Agrawal. Prediction of seebeck coefficient for compounds without restriction to fixed stoichiometry: A machine learning approach. *Journal of Computational Chemistry*, 39(4):191–202, 2018.
- [11] HM Yuan, SH Han, R Hu, WY Jiao, MK Li, HJ Liu, and Y Fang. Machine learning for accelerated prediction of the seebeck coefficient at arbitrary carrier concentration. *Materials Today Physics*, 25:100706, 2022.
- [12] Nikhil K Barua and Holger Kleinke. Machine learning predictions of thermopower for thermoelectric material screening. ACS Applied Energy Materials, 2025.
- [13] Abhishek Tewari, Siddharth Dixit, Niteesh Sahni, and Stéphane PA Bordas. Machine learning approaches to identify and design low thermal conductivity oxides for thermoelectric applications. *Data-Centric Engineering*, 1: e8, 2020.
- [14] Xinming Wang, Shuming Zeng, Zhuchi Wang, and Jun Ni. Identification of crystalline materials with ultra-low thermal conductivity based on machine learning study. *The Journal of Physical Chemistry C*, 124(16):8488–8495, 2020.
- [15] Nikhil K Barua, Evan Hall, Yifei Cheng, Anton O Oliynyk, and Holger Kleinke. Interpretable machine learning model on thermal conductivity using publicly available datasets and our internal lab dataset. *Chemistry of Materials*, 36(14):7089–7100, 2024.
- [16] Zihe Li, Mengke Li, Yufeng Luo, Haibin Cao, Huijun Liu, and Ying Fang. Machine learning for accelerated prediction of lattice thermal conductivity at arbitrary temperature. *Digital Discovery*, 4(1):204–210, 2025.
- [17] Jun Mao, Yixuan Wu, Shaowei Song, Qing Zhu, Jing Shuai, Zihang Liu, Yanzhong Pei, and Zhifeng Ren. Defect engineering for realizing high thermoelectric performance in n-type Mg₃Sb₂-based materials. *ACS Energy Letters*, 2(10):2245–2250, 2017.
- [18] Yu Zhang, Zhi Li, Saurabh Singh, Amin Nozariasbmarz, Wenjie Li, Aziz Genç, Yi Xia, Luyao Zheng, Seng Huat Lee, Sumanta Kumar Karan, et al. Defect-engineering-stabilized AgSbTe₂ with high thermoelectric performance. *Advanced Materials*, 35(11):2208994, 2023.
- [19] Yanling Pei, Gangjian Tan, Dan Feng, Lei Zheng, Qing Tan, Xiaobing Xie, Shengkai Gong, Yue Chen, Jing-Feng Li, Jiaqing He, et al. Integrating band structure engineering with all-scale hierarchical structuring for high thermoelectric performance in PbTe system. *Advanced Energy Materials*, 7(3):1601450, 2017.
- [20] Hongyao Xie, Yukun Liu, Yinying Zhang, Shiqiang Hao, Zhi Li, Matthew Cheng, Songting Cai, G Jeffrey Snyder, Christopher Wolverton, Ctirad Uher, et al. High Thermoelectric Performance in Chalcopyrite Cu_{1-x}Ag_x GaTe₂–ZnTe: Nontrivial Band Structure and Dynamic Doping Effect. *Journal of the American Chemical Society*, 144(20):9113–9125, 2022.
- [21] Qingtang Zhang, Pan Ying, Aftab Farrukh, Yaru Gong, Jizi Liu, Xinqi Huang, Di Li, Meiyu Wang, Guang Chen, and Guodong Tang. High wide-temperature-range thermoelectric performance in GeTe through heteronanostructuring. Acta Materialia, 276:120132, 2024.
- [22] Yun Zheng, Qiang Zhang, Xianli Su, Hongyao Xie, Shengcheng Shu, Tianle Chen, Gangjian Tan, Yonggao Yan, Xinfeng Tang, Ctirad Uher, et al. Mechanically robust BiSbTe alloys with superior thermoelectric performance: a case study of stable hierarchical nanostructured thermoelectric materials. *Advanced Energy Materials*, 5(5): 1401391, 2015.
- [23] Glen A Slack, DM Rowe, et al. CRC handbook of thermoelectrics, 1995.
- [24] GS Nolas, DT Morelli, and Terry M Tritt. Skutterudites: A phonon-glass-electron crystal approach to advanced thermoelectric energy conversion applications. *Annual Review of Materials Science*, 29(1):89–116, 1999.
- [25] Toshiro Takabatake, Koichiro Suekuni, Tsuneyoshi Nakayama, and Eiji Kaneshita. Phonon-glass electron-crystal thermoelectric clathrates: Experiments and theory. *Reviews of Modern Physics*, 86(2):669–716, 2014.
- [26] G Jeffrey Snyder, Mogens Christensen, Eiji Nishibori, Thierry Caillat, and Bo Brummerstedt Iversen. Disordered zinc in Zn₄Sb₃ with phonon-glass and electron-crystal thermoelectric properties. *Nature Materials*, 3(7):458–463, 2004.
- [27] Yukari Katsura, Masaya Kumagai, Tomoya Mato, Yu Takada, Yuki Ando, Erina Fujita, Fumikazu Hosono, Eiji Koyama, Farhan Mudasar, Ton Nu Thanh Phuong, et al. Starrydata: from published plots to shared materials data. *Science and Technology of Advanced Materials: Methods*, 5(1):2506976, 2025.

- [28] Logan Ward, Ankit Agrawal, Alok Choudhary, and Christopher Wolverton. A general-purpose machine learning framework for predicting properties of inorganic materials. *npj Computational Materials*, 2(1):1–7, 2016.
- [29] Anubhav Jain, Shyue Ping Ong, Geoffroy Hautier, Wei Chen, William Davidson Richards, Stephen Dacek, Shreyas Cholia, Dan Gunter, David Skinner, Gerbrand Ceder, et al. Commentary: The Materials Project: A materials genome approach to accelerating materials innovation. *APL Materials*, 1(1), 2013.
- [30] Hyun-Sik Kim, Zachary M Gibbs, Yinglu Tang, Heng Wang, and G Jeffrey Snyder. Characterization of Lorenz number with Seebeck coefficient measurement. *APL Materials*, 3(4), 2015.
- [31] Huili Liu, Xun Shi, Fangfang Xu, Linlin Zhang, Wenqing Zhang, Lidong Chen, Qiang Li, Ctirad Uher, Tristan Day, and G Jeffrey Snyder. Copper ion liquid-like thermoelectrics. *Nature materials*, 11(5):422–425, 2012.
- [32] Lisha Xue, Weixia Shen, Zhuangfei Zhang, Manjie Shen, Wenting Ji, Chao Fang, Yuewen Zhang, and Xiaopeng Jia. Off-stoichiometry effects on the thermoelectric properties of $Cu_{2+\delta}Se$ (-0.1 $\leq \delta \leq$ 0.05) compounds synthesized by a high-pressure and high-temperature method. *CrystEngComm*, 22(4):695–700, 2020.
- [33] Shanyu Wang, Wenjie Xie, Han Li, and Xinfeng Tang. Enhanced performances of melt spun Bi₂(Te,Se)₃ for n-type thermoelectric legs. *Intermetallics*, 19(7):1024–1031, 2011.
- [34] Bing Sun, Xiaopeng Jia, Dexuan Huo, Hairui Sun, Yuewen Zhang, Binwu Liu, Haiqiang Liu, Lingjiao Kong, Baomin Liu, and Hongan Ma. Effect of high-temperature and high-pressure processing on the structure and thermoelectric properties of clathrate Ba₈Ga₁₆Ge₃₀. The Journal of Physical Chemistry C, 120(18):10104–10110, 2016.
- [35] Adul Harnwunggmoung, Ken Kurosaki, Hiroaki Muta, and Shinsuke Yamanaka. High-temperature thermoelectric properties of thallium-filled skutterudites. *Applied Physics Letters*, 96(20), 2010.
- [36] Eun Bin Kim, Peyala Dharmaiah, Kap-Ho Lee, Chul-Hee Lee, Jong-Hyeon Lee, Jae-Kyo Yang, Dae-Hwan Jang, Dong-Soo Kim, and Soon-Jik Hong. Enhanced thermoelectric properties of Bi_{0.5}Sb_{1.5}Te₃ composites with in-situ formed senarmontite Sb₂O₃ nanophase. *Journal of Alloys and Compounds*, 777:703–711, 2019.
- [37] Sora-at Tanusilp, Suphagrid Wongprakarn, Pinit Kidkhunthod, Yuji Ohishi, Hiroaki Muta, and Ken Kurosaki. Beneficial influence of iodine substitution on the thermoelectric properties of Mo₃Sb₇. *Journal of Applied Physics*, 127(10), 2020.
- [38] Wenjing Xu, Zhongwei Zhang, Chengyan Liu, Jie Gao, Zhenyuan Ye, Chunguang Chen, Ying Peng, Xiaobo Bai, and Lei Miao. Substantial thermoelectric enhancement achieved by manipulating the band structure and dislocations in Ag and La co-doped SnTe. *Journal of Advanced Ceramics*, 10(4):860–870, 2021.
- [39] Mohamed S El-Asfoury, Shaban M Abdou, and Ahmed Nassef. Unraveling the thermoelectric performance of Bismuth Antimony/graphene nanocomposite synthesized by spark plasma extrusion. *Journal of Alloys and Compounds*, 887:161399, 2021.
- [40] Xin Liang and Chuang Chen. Ductile inorganic amorphous/crystalline composite Ag₄TeS with phonon-glass electron-crystal transport behavior and excellent stability of high thermoelectric performance on plastic deformation. *Acta Materialia*, 218:117231, 2021.
- [41] Jinfeng Dong, Fu-Hua Sun, Huaichao Tang, Jun Pei, Hua-Lu Zhuang, Hai-Hua Hu, Bo-Ping Zhang, Yu Pan, and Jing-Feng Li. Medium-temperature thermoelectric GeTe: vacancy suppression and band structure engineering leading to high performance. *Energy & Environmental Science*, 12(4):1396–1403, 2019.
- [42] Oliver Falkenbach, Andreas Schmitz, Torben Dankwort, Guenter Koch, Lorenz Kienle, Eckhard Mueller, and Sabine Schlecht. Tin Telluride-Based Nanocomposites of the Type AgSn_mBiTe_{2+m} (BTST-m) as Effective Lead-Free Thermoelectric Materials. *Chemistry of Materials*, 27(21):7296–7305, 2015.
- [43] Ying Lei, Wensheng Gao, Rui Zheng, Yu Li, Wen Chen, Libo Zhang, Rundong Wan, Hongwei Zhou, Zhiyuan Liu, and Paul K Chu. Ultrafast synthesis of Te-doped CoSb₃ with excellent thermoelectric properties. *ACS Applied Energy Materials*, 2(6):4477–4485, 2019.
- [44] Xun Shi, Jiong Yang, James R Salvador, Miaofang Chi, Jung Y Cho, Hsin Wang, Shengqiang Bai, Jihui Yang, Wenqing Zhang, and Lidong Chen. Multiple-filled skutterudites: high thermoelectric figure of merit through separately optimizing electrical and thermal transports. *Journal of the American Chemical Society*, 133(20): 7837–7846, 2011.
- [45] T Caillat, A Borshchevsky, and J-P Fleurial. Properties of single crystalline semiconducting CoSb₃. *Journal of Applied Physics*, 80(8):4442–4449, 1996.
- [46] Kwan-Ho Park, Won-Seon Seo, Dong-Kil Shin, and Il-Ho Kim. Thermoelectric properties of Yb-filled CoSb₃ skutterudites. *Journal of the Korean Physical Society*, 65(4):491–495, 2014.

- [47] Y Dou, J Li, Y Xie, X Wu, L Hu, F Liu, W Ao, Y Liu, and C Zhang. Lone-pair engineering: Achieving ultralow lattice thermal conductivity and enhanced thermoelectric performance in Al-doped GeTe-based alloys. *Materials Today Physics*, 20:100497, 2021.
- [48] Zihang Liu, Jifeng Sun, Jun Mao, Hangtian Zhu, Wuyang Ren, Jingchao Zhou, Zhiming Wang, David J Singh, Jiehe Sui, Ching-Wu Chu, et al. Phase-transition temperature suppression to achieve cubic GeTe and high thermoelectric performance by Bi and Mn codoping. *Proceedings of the National Academy of Sciences*, 115(21): 5332–5337, 2018.
- [49] Juan Li, Zhiwei Chen, Xinyue Zhang, Hulei Yu, Zihua Wu, Huaqing Xie, Yue Chen, and Yanzhong Pei. Simultaneous optimization of carrier concentration and alloy scattering for ultrahigh performance GeTe thermoelectrics. *Advanced Science*, 4(12):1700341, 2017.
- [50] Lihua Wu, Xin Li, Shanyu Wang, Tiansong Zhang, Jiong Yang, Wenqing Zhang, Lidong Chen, and Jihui Yang. Resonant level-induced high thermoelectric response in indium-doped GeTe. NPG Asia Materials, 9(1):e343–e343, 2017
- [51] EM Levin, MF Besser, and Riley Hanus. Electronic and thermal transport in GeTe: A versatile base for thermoelectric materials. *Journal of Applied Physics*, 114(8), 2013.
- [52] Min Hong, Zhi-Gang Chen, Lei Yang, Yi-Chao Zou, Matthew S Dargusch, Hao Wang, and Jin Zou. Realizing zT of 2.3 in $Ge_{1-x-y}Sb_xIn_y$ Te via reducing the phase-transition temperature and introducing resonant energy doping. *Advanced materials*, 30(11):1705942, 2018.
- [53] Juan Li, Xinyue Zhang, Siqi Lin, Zhiwei Chen, and Yanzhong Pei. Realizing the high thermoelectric performance of GeTe by Sb-doping and Se-alloying. *Chemistry of Materials*, 29(2):605–611, 2017.
- [54] Mohsin Saleemi, A Ruditskiy, MS Toprak, Marian Stingaciu, Mats Johnsson, I Kretzschmar, A Jacquot, M Jägle, and Mamoun Muhammed. Evaluation of the structure and transport properties of nanostructured antimony telluride (Sb₂Te₃). *Journal of Electronic Materials*, 43(6):1927–1932, 2014.
- [55] LP Hu, TJ Zhu, XQ Yue, XH Liu, YG Wang, ZJ Xu, and XB Zhao. Enhanced figure of merit in antimony telluride thermoelectric materials by In–Ag co-alloying for mid-temperature power generation. *Acta Materialia*, 85:270–278, 2015.
- [56] Heng Quan Yang, Lei Miao, Cheng Yan Liu, Chao Li, Sawao Honda, Yuji Iwamoto, Rong Huang, and Sakae Tanemura. A facile surfactant-assisted reflux method for the synthesis of single-crystalline Sb₂Te₃ nanostructures with enhanced thermoelectric performance. *ACS Applied Materials & Interfaces*, 7(26):14263–14271, 2015.
- [57] Guo-Hui Dong, Ying-Jie Zhu, and Li-Dong Chen. Microwave-assisted rapid synthesis of Sb₂Te₃ nanosheets and thermoelectric properties of bulk samples prepared by spark plasma sintering. *Journal of Materials Chemistry*, 20 (10):1976–1981, 2010.
- [58] John Dagdelen, Alexander Dunn, Sanghoon Lee, Nicholas Walker, Andrew S Rosen, Gerbrand Ceder, Kristin A Persson, and Anubhav Jain. Structured information extraction from scientific text with large language models. *Nature Communications*, 15(1):1418, 2024.
- [59] Suman Itani, Yibo Zhang, and Jiadong Zang. Large language model-driven database for thermoelectric materials. *Computational Materials Science*, 253:113855, 2025.
- [60] Hongxu An, Dongyang Wang, and Wenke He. Thermoelectric properties of AgBiS₂: Unveiling the origin of ultra-low lattice thermal conductivity and optimization strategies for electrical performance. *Applied Physics Letters*, 127(14), 2025.
- [61] Dean Hobbis, Kaya Wei, Hsin Wang, Joshua Martin, and George S Nolas. Synthesis, structure, Te alloying, and physical properties of CuSbS₂. *Inorganic Chemistry*, 56(22):14040–14044, 2017.
- [62] Haonan Shi, Changrong Guo, Bingchao Qin, Guangtao Wang, Dongyang Wang, and Li-Dong Zhao. A promising thermoelectrics In₄SnSe₄ with a wide bandgap and cubic structure composited by layered SnSe and In₄Se₃. *Journal of Materiomics*, 8(5):982–991, 2022.
- [63] Alex Zevalkink, Gregory Pomrehn, Yoshiki Takagiwa, Jessica Swallow, and G Jeffrey Snyder. Thermoelectric Properties and Electronic Structure of the Zintl-Phase Sr₃AlSb₃. *ChemSusChem*, 6(12):2316–2321, 2013.
- [64] Hua Lin, Hong Chen, Ni Ma, Yu-Jun Zheng, Jin-Ni Shen, Ju-Song Yu, Xin-Tao Wu, and Li-Ming Wu. Syntheses, structures, and thermoelectric properties of ternary tellurides: RECuTe₂ (RE=Tb-Er). *Inorganic Chemistry Frontiers*, 4(8):1273–1280, 2017.